Colloid Polym Sci 278:37–47 (2000)

ORIGINAL CONTRIBUTION

Rheological behavior in the didodecyldimethylammonium bromide/water system

J.F.A. Soltero
F. Bautista
E. Pecina
J.E. Puig
O. Manero
Z. Proverbio
P.C. Schulz

Received: 4 January 1999
Accepted in revised form: 1 September 1999

J.F.A. Soltero (✉) · F. Bautista
E. Pecina · J.E. Puig
Departamento de Ingenieria Química
Universidad de Guadalajara
Boul. M. García Barragán 1451
Guadalajara, Jal. 44430, Mexico

O. Manero
Instituto de Investigaciones en Materiales
Universidad Nacional Autónoma
de México
Apdo. Postal 70-360
México, D.F. 04510, Mexico

Z. Proverbio · P.C. Schulz
Departamento de Química
e Ingeniería Química
Universidad Nacional del Sur
Bahía Blanca 8000, Argentina

Abstract The phase behavior in the dilute region of the didodecyldimethylammonium bromide (DDAB)/water system is studied with a battery of techniques. The critical vesicle concentration (cvc), measured by tensiometry, conductimetry, ion-selective-electrode potentiometry and dye solubilization, is similar to the value reported in the literature. Moreover, the combination of surfactant-ion-selective-electrode and bromide-ion-selective-electrode potentiometry indicates that the vesicles are substantially ionized ($\alpha \approx 0.5$) in the proximity of the cvc. The transition from small unilamellar vesicles to larger multilamellar liposomes was detected at 0.2 wt% by viscometry, conductimetry and dye solubilization measurements. The rheology of the DDAB/water system was studied as a function of surfactant concentration and temperature. Non-Newtonian behavior, viscoelasticity, yield stresses and time-dependent flow behavior were observed. Maxima and minima in the dynamic moduli and in conductivity are related to structural changes and phase transitions. Moreover, in time-dependent shear flow, the microstructure is modified and the rheological response shifts from thixotropic to antithixotropic or vice versa, depending on the DDAB concentration and the level and duration of the final applied stress. The conductivity behavior in the Lam_1 phase region can be qualitatively explained by the capillary superconductivity theory. This conductivity behavior occurs when the thickness of the aqueous lamella is of the same order of magnitude as the Debye length.

Key words Vesicles · Lamellar liquid crystals · Viscoelasticity · Thixotropic-antithixotropic

Introduction

Didodecyldimethylammonium bromide (DDAB) is a double-tail cationic surfactant, whose phase behavior in water and in water/oil mixtures has been studied in detail [1–7]. In water, DDAB forms vesicles but not micelles above its critical vesicle concentration (cvc) of 6.5×10^{-4} wt% [1]. Above 4 wt% and up to 30 wt%, a highly swollen lamellar phase (Lam_1) forms at room temperature [3]. Another single lamellar phase (Lam_2) is observed between 85 and 89 wt% DDAB. In-between, there is a wide two-phase region. Both lamellar phases change into an isotropic phase upon increasing the temperature [7], although more recently it has been reported that the biphasic (Lam_1 + Lam_2) region has a critical point at 74 °C and 62.2 wt% surfactant, above which the Lam_2 phase prevails up to about 100 °C [8, 9].

The rheology of DDAB-based microstructured fluids has been scarcely studied. Matsumoto et al. [1] performed a morphological and rheological study at 25 °C of DDAB/water mixtures up to 40 wt% surfactant concentration. Steady-shear measurements reveal Newtonian

behavior at DDAB concentrations below 1 wt% and non-Newtonian behavior at higher concentrations where the zero-shear-rate viscosity (η_0) increases in a non monotonous fashion with increasing surfactant concentration. Oscillatory measurements, performed at shear-strain deformations within the linear viscoelastic region ($\gamma \approx 3\%$), show that the samples behave as "weak gels", i.e., their dynamic moduli (G' and G'') are independent of frequency and $G' \gg G''$ [10]. Moreover, Matsumoto et al. [1] reported that the dynamic moduli and the shear viscosity (η) go through maxima at 3 wt% and between 15 and 20 wt% DDAB. This anomalous rheological behavior was explained in terms of structural changes occurring at those concentrations; however, the whole phase diagram was not covered and measurements were performed only at room temperature.

In this paper, the rheological properties of the DDAB/water system are reported as a function of surfactant concentration and temperature. The phase behavior at low concentrations and the degree of ionization of the vesicles are investigated by a battery of techniques. The relationship between phase behavior and rheological properties is examined. Moreover, the conductivity behavior in the Lam_1 region is explained in terms of the capillary superconductivity theory [11].

Experimental

DDAB (Kodak) with a purity higher than 99% was recrystallized first from a 50/50 (v/v) acetone/ethyl ether mixture and was then from ethyl acetate and was dried in a vacuum oven. Samples were prepared by adding water to the dried surfactant, then they were heated, homogenized and allowed to reach equilibrium for at least 1 week at 25 ± 0.1 °C.

Conductivity was measured at 25 °C and 1000 Hz with a Labcraft CMS 064-774 conductimeter and an immersion cell with a constant of 1 cm^{-1}. Turbidity was measured at 600 nm in quartz cells with path lengths of 0.5 cm using a Perkin Elmer Lambda II spectrophotometer. Solubilization of Sudan III (99% pure from Fluka) in the aggregates was followed with a Spectronic 20 spectrophotometer at a wavelength of 490 nm. The critical aggregation concentration was also detected by adding a drop of a dilute aqueous solution of Rhodamine 6G (99% + purity from Carlo Erba) to DDAB/water samples. This dye changes its color and fluorescence (from fluorescent orange to non fluorescent sensitive red) when aggregates form [13]. The change in color can be detected by eye.

Ion-selective-electrode potentiometry was conducted using a CRIBBAB voltmeter with an Orion 9435BN Br^--selective electrode and a homemade surfactant-ion-selective (DDA^+) electrode. The DDA^+-selective electrode was made as follows. Dilute equimolar aqueous solutions of DDAB and sodium dodecyl sulfate (99% pure from Aldrich) were mixed to produce a complex that precipitates. This precipitate was filtered and washed several times with doubly distilled water and was then dried. Next, 0.3 g of this complex, 0.3 g poly(vinyl chloride) (PVC) and 0.06 g dibutyl phthalate (used as a plasticizer) were dissolved in 3 ml tetrahydrofuran (Merck). This solution was loaded in a petri dish and allowed to dry to yield a thin membrane film; this was glued to the end of a PVC tube with tetrahydrofuran. Then the tube was filled with an aqueous solution of 0.1 mM NaBr and 1 mM DDAB, and a silver electrode (which acts as the internal electrode) was introduced into the tube. The reference electrode for both the Br^-- and the DDA^+-selective electrodes was an Orion saturated calomel electrode.

Rheological properties were measured with a Carri-Med C50 controlled-stress rheometer and cone-and-plate-geometry (0.035 rad and 4 cm) and with a Rheometrics RDS II mechanical spectrometer and cone-and-plate-geometry (0.1 rad and 2.5 cm). Since the domain structure of DDAB liquid-crystalline samples is quite sensitive to shear deformation history, samples were carefully loaded on the rheometer plate with a spatula and then the cone was slowly lowered. To prevent changes in composition by water evaporation during measurements, a chamber containing wetted sponges was placed around the cone-and-plate fixture. The viscosity of the dilute solutions was measured at 25 °C with a calibrated Cannon Fenske no. 50 viscometer.

Results

The surface tension and absorbance due to Sudan III solubilization is shown in Fig. 1 as a function of DDAB concentration. The slope of the surface tension curve changes abruptly at 0.086 mM (4×10^{-3} wt%) and at about 0.86 mM (4×10^{-2} wt%); in the latter case, the surface tension remains constant with increasing DDAB concentration. Sudan III solubilization absorbance is small in dilute samples but increases abruptly with DDAB concentration at about 0.043 mM (2×10^{-3} wt%). A second transition, signaled by another sudden increase in absorbance, is detected at 0.63 mM (2.9×10^{-2} wt%). The turbidity measured at 600 nm (not shown) increases rapidly with DDAB concentration above 0.023 mM (1.08×10^{-3} wt%). The first transition was also detected visually at 0.05 mM (2.3×10^{-3} wt%) by observing the color change of Rhodamine 6G in DDAB solutions.

The plot of conductivity versus DDAB concentration exhibits two transitions at low concentrations as evidenced by changes in the slope: one at about 0.018 mM (8.5×10^{-4} wt%) and the other at 0.43 mM (2×10^{-2} wt%) (Fig. 2). To analyze further the conductivity data, the equivalent conductivity, Λ, as a function of $\sqrt{c}$ and

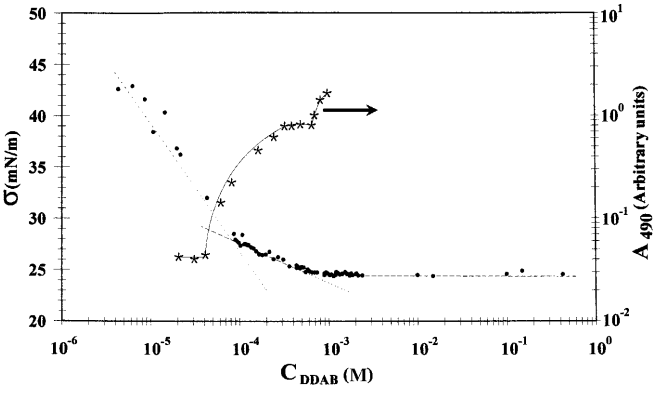

Fig. 1 Surface tension and Sudan III solubilization absorbance, measured at 490 nm, versus didodecyldimethylammonium bromide (*DDAB*) concentration

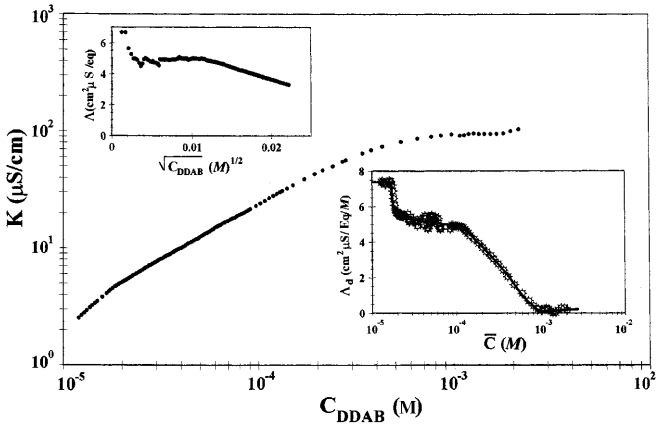

Fig. 2 Electrical conductivity as a function of DDAB concentration. *Insets*: equivalent conductivity, Λ, versus square root of DDAB concentration and differential equivalent conductivity, Λ_d, versus $\bar{c}$

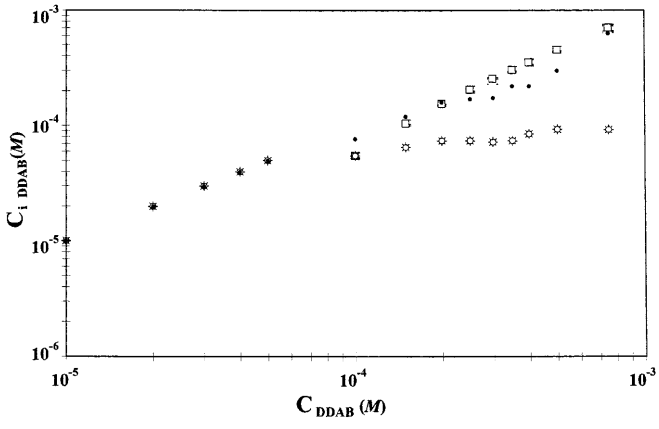

Fig. 3 Concentrations of free Br^- (●), free DDA^+ (✲), and aggregated DDAB (□)

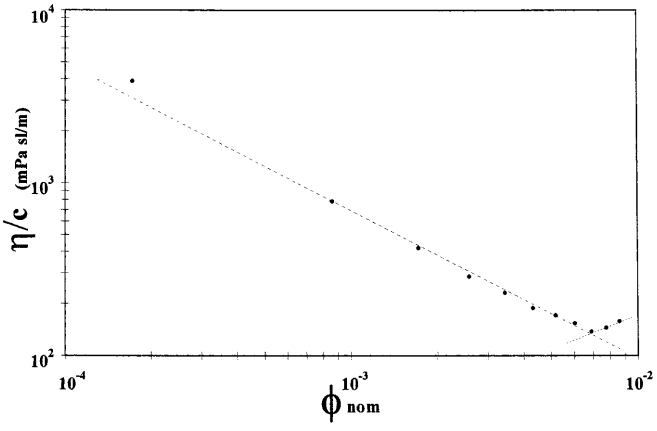

Fig. 4 Relative viscosity as a function of nominal volume fraction

Table 1 Concentrations where transitions were detected by the different methods

Method	First transition (mM × 10^2)	Second transition (mM × 10^2)
Electrical conductivity	1.7–1.9	43
Equivalent conductivity	3.0	–
Differential equivalent conductivity	1.7–1.9	43
Surface tension	7.0–8.6	86
Ion-selective electrodes	5.0	40–50
Sudan III solubilization	4.3	63
Turbidimetry	2.3	–
Rhodamine 6G	5.0	–
Viscometry	–	88

the differential equivalent conductivity, Λ_d ($\equiv 1000\Delta\kappa/\Delta c$), versus $\bar{c}$ ($\equiv[c_n + c_{n-1}]/2$), are shown in the insets of Fig. 2. Λ drops abruptly with concentration up to the first transition, where a small minimum followed by a plateau is observed; then it drops with increasing DDAB concentration with no evidence of the second transition from dye solubilization and conductivity measurements. Λ_d, on the other hand, exhibits two plateaus at low and high concentrations and two drops separated by a zone with a small slope at intermediate concentrations. The drops in Λ_d occur at the same concentrations where the slope of the conductivity plot changes.

The concentrations of free $Br^-$and DDA^+ and of aggregated DDA^+ (on a monomer basis), obtained from ion-selective-electrode measurements, are shown in Fig. 3. Free-ion and aggregated-ion concentrations and the degree of ionization were calculated with a procedure described elsewhere [12] with the assumption that the aggregates do not contribute significantly to the ionic strength of the solution [13]. Both DDA^+ and Br^- concentrations increase up to 0.05 mM, where the aggregates form, then the concentration of free DDA^+ becomes almost constant, whereas that of free Br^- keeps increasing, which indicates that the aggregates are strongly ionized.

The relative viscosity, η/c, versus the nominal volume fraction, $\phi_{nom}(\equiv c\bar{V}/1000)$ is shown in a log-log form in Fig. 4 c is the DDAB molar concentration above the cvc and $\bar{V}$ (+796.9 cm^3/mol) is the surfactant molar volume. The latter was calculated using the model of Gruen [14] to estimate the volume of the hydrocarbon groups and with literature data for the volume of the nitrogen atom in an alkylammonium group [15]. The relative viscosity decreases with volume fraction up to $\phi_{nom} = 0.0074$ ($c_{DDAB} = 8.81$ mM). Then the slope becomes steeper, suggesting a structural change at this concentration. The concentrations at which the two transitions were detected by the different techniques employed as well as literature values are reported in Table 1. Note that the concentrations where the transi-

tions are observed vary slightly depending on the method used.

Strain-deformation sweeps (not shown) were performed as a function of DDAB concentration at 25 °C and at a constant frequency of 10 rad/s to detect the linear viscoelastic region. This region, defined here as the region where the elastic modulus (G′) is independent of the applied strain level, is restricted to small values. The critical strain deformation, γ_c, decreases with increasing DDAB concentration: γ_c is about 4% for the 15 wt% sample and only 2% for the 30 wt% sample. In the biphasic ($Lam_1 + Lam_2$) region, $\gamma_c \leq 2\%$ and in the Lam_2 phase, $\gamma_c \leq 0.5\%$. All the dynamics experiments reported here were performed in the linear viscoelastic regime, except when indicated otherwise.

The creep flow and the creep recovery of a 20 wt% DDAB sample are depicted in Fig. 5. Curve A in Fig. 5 shows the compliance, *J*, as a function of time when the applied stress is small ($\tau = 1$ Pa). The deformation curve in this case is similar to that of viscoelastic solids, such as asphalt, melted metals and cross-linked polymers [16], in which the deformation becomes constant with time after the initial elastic response; when the stress is released, the deformation immediately relaxes. On the other hand, when a larger stress is applied ($\tau = 20$ Pa), the material behaves as a viscoelastic liquid, i.e., an elastic response at very short times (less than 2 s), followed by flow up to a steady state, which is reached after about 100 s (curve B in Fig. 5). When the stress is removed, the sample relaxes immediately to a finite deformation value, then it relaxes more slowly. These results suggest that the sample has a yield stress (τ_y), i.e., it has a Bingham plastic like behavior [16]. τ_y was determined by performing creep experiments. Samples at all concentrations exhibit yield stresses. The inset depicts in semilogarithmic form the compliance, *J*, as a function of time for various stresses.

τ_y is shown as a function of DDAB concentration in Fig. 6. The yield stresses are small in the low-concentration biphasic region and larger in the Lam_1 region; in the latter, τ_y increases with DDAB concentration, then it goes through a maximum at 20 wt% and a minimum at the phase boundary with the biphasic ($Lam_1 + Lam_2$) region, and then increases again up to the phase boundary with the Lam_2 region.

Frequency sweeps performed in a controlled-stress rheometer at stress values below and above the measured τ_y of the 20 wt% liquid-crystalline sample ($\tau_y \approx 5$ Pa) are shown in Fig. 7. When the applied stress ($\tau = 2$ Pa) is smaller than τ_y, the material behaves as a weak gel (Fig. 7A). By contrast, when the applied stress ($\tau = 10$ Pa) exceeds τ_y (unsteady-state conditions), a viscoelastic response is observed, where G′ and G increase with ω in the terminal region with slopes close to those reported for flexible polymer solutions [16]. Also, a crossover between G′ and G″ at a frequency equal to the reciprocal of the largest relaxation time of the system is observed (Fig. 7B). Above this characteristic frequency, G′ becomes larger than G″.

The dynamic moduli (G′ and G″) measured at 10 rad/s and the electrical conductivity are shown in Fig. 8 as a function of DDAB concentration. Both dynamic moduli exhibit maxima at 3, 20 and about 90 wt% DDAB. Matsumoto et al. [1] also reported maxima in G′ and G″ at 3 and 20 wt% DDAB. Notice also that the samples in the Lam_2 region have larger moduli than those in the Lam_1 region. The electrical conductivity, in turn, increases with DDAB concentration up to a maximum at 10 wt%; then it decreases and goes through a minimum at 25 wt%, after which it increases again with surfactant concentration. A shallow maximum is also observed near the phase boundary with the Lam_2 region. The conductivity could not be measured at higher concentrations due to the high viscosity of the samples, which makes the insertion of

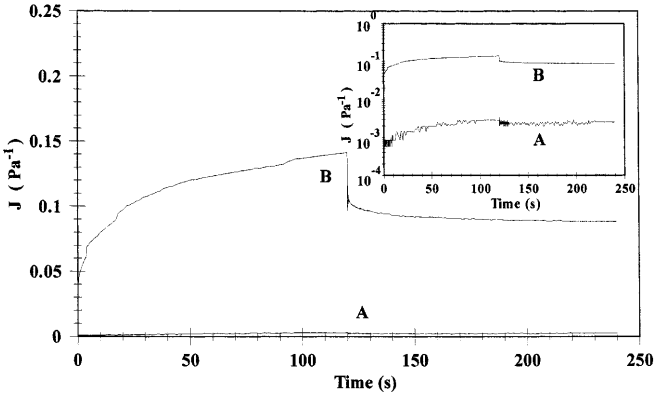

Fig. 5 Compliance versus time for creep flow and creep recovery of a 20 wt% DDAB sample, when the applied stress is 1 Pa (*A*) and 20 Pa (*B*). *Inset*: plot of ln *J* as a function of time for two values of the stress 1 Pa (*A*) and 20 Pa (*B*)

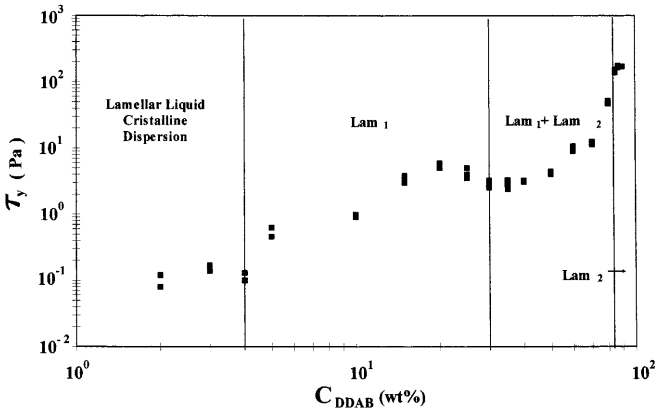

Fig. 6 Yield stress as a function of DDAB concentration

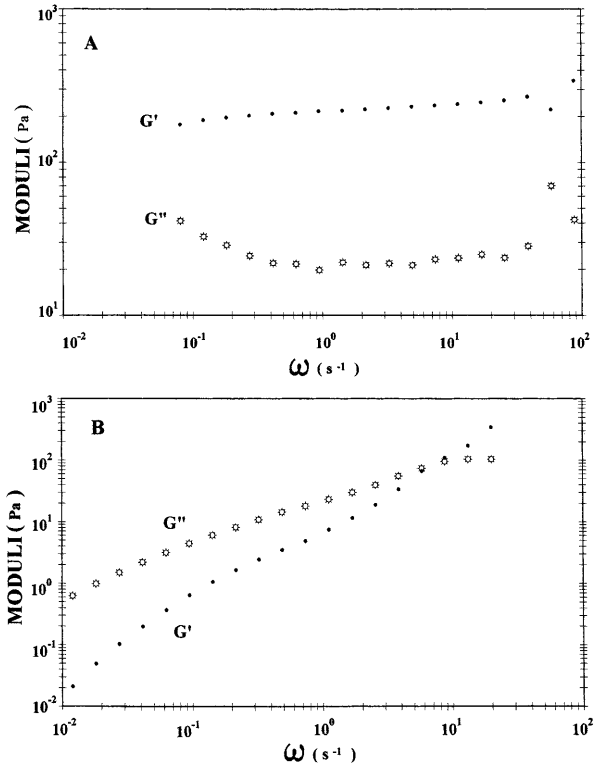

Fig. 7 Frequency sweeps performed in a controlled-stress rheometer on a 20 wt% DDAB lamellar liquid-crystalline sample when the applied stress is **A** 2 Pa and **B** 10 Pa: elastic moduli (●) and loss moduli (✡)

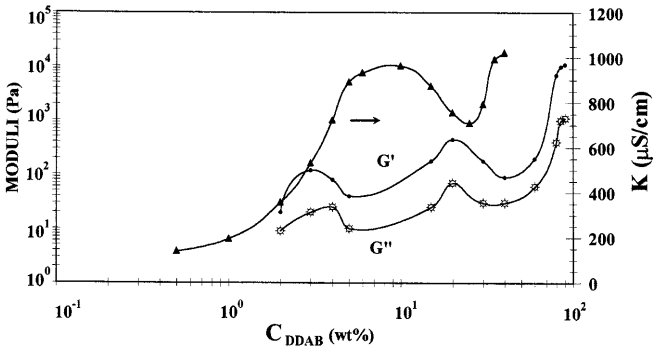

Fig. 8 Elastic (●) and viscous (✡) moduli and electrical conductivity (▲) as a function of DDAB concentration

the cell and the complete covering of the electrodes difficult.

Temperature sweeps performed at 10 rad/s are shown in Fig. 9. The 20 wt% sample, which is in the Lam_1 region, exhibits a predominately elastic response, i.e., $G' > G''$, in the whole temperature range. Moreover, an inflexion in both G' and G'' is detected at about 20 °C, which corresponds to the Kraft temperature (T_k) of DDAB in water at this concentration. The 90 wt% sample, which is in the Lam_2 region, exhibits very large moduli at temperatures below T_k and a sharp drop in both moduli at T_k. Above T_k, G' is larger than G'' and both are fairly independent of temperature, although a small inflexion is detected at about 55 °C.

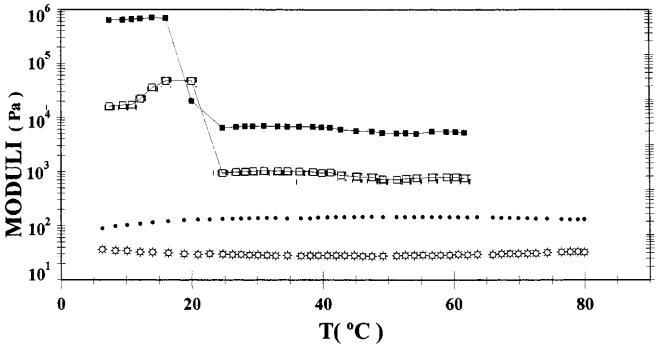

Fig. 9 Temperature sweeps performed at 10 rad/s on a 20 wt% sample, elastic (●) and loss (✡) moduli, and on a 90 wt% sample, elastic (■) and loss (□) moduli

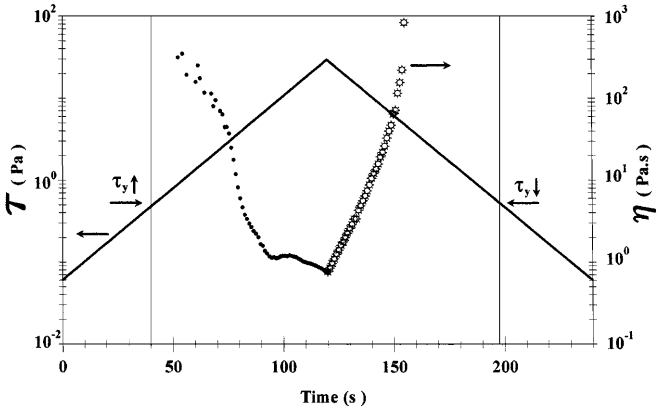

Fig. 10 Applied stress and shear viscosity as a function of time in an exponentially increasing and decreasing stress program applied to a 10 wt% DDAB sample

The stress versus time and the viscosity response of a 10 wt% DDAB sample in an exponentially increasing and decreasing stress cycle are depicted in Fig. 10. In this experiment, performed at unsteady-state conditions, the sample is subjected to an exponentially increasing stress ramp at a predetermined rate and then to an exponentially decreasing stress ramp at the same rate. The viscosity of the sample drops rapidly with increasing stress and then it increases in the decreasing stress ramp as expected. Notice, however, that the viscosity in the decreasing ramp is higher than that in the increasing ramp, i.e., the sample exhibits antithixotropy. Moreover, there is no flow during the increasing ramp unless a minimum stress has been applied, i.e., an apparent yield stress is observed (indicated as $\tau_y^{\Uparrow}$ in Fig. 10) and until the stress drops below certain value in the descending

mode ($\tau_y^{\Downarrow}$). For most of the samples examined here, $\tau_y^{\Uparrow}$ and $\tau_y^{\Downarrow}$ are not equal.

Figure 11 shows the viscosity as a function of shear rate in exponentially increasing and decreasing stress cycles imposed at unsteady-state conditions on samples located in the different regions of the phase diagram. In the 1 wt% DDAB sample, yield stresses and thixotropic loops are observed as the stress is increased from 0.06 to 1 Pa in 2 min; notice that $\tau_y^{\Uparrow}$ is larger than $\tau_y^{\Downarrow}$ (Fig. 11A). When the final stress is increased from 1 to 2 Pa, a larger thixotropic area is observed (not shown) [17]. The viscosity exhibits a power-law behavior for shear rates ranging from 0.1 to 1 s^{-1} to approximately 10 s^{-1}, after which a region of almost constant viscosity is observed: this is in contrast to the conclusion of Matsumoto et al. [1] that the system is Newtonian at this concentration.

In the concentration range where the first maximum in the viscoelastic properties is observed (3–4 wt%), the rheological behavior changes dramatically. In this case, antithixotropic loops are observed over most of the shear-rate range examined when the stress is increased from 0.06 to 5 Pa and now $\tau_y^{\Uparrow}$ is smaller than $\tau_y^{\Downarrow}$ (Fig. 11B). In the ascending mode, two power-law regions separated by a nearly constant viscosity region are observed, whereas a single power-law behavior is observed in the descending mode. This behavior is also detected in the single Lam_1 region in samples with concentrations up to 12–13 wt% DDAB as well as in Aerosol OT (AOT)/water liquid-crystalline dispersions [18].

In the 15–20 wt% concentration range, where the second maximum in the viscoelastic properties is observed, the rheological behavior is almost antithixotropic within the applied stress levels (0.06–300 Pa) (Fig. 11C). There is not a single power-law region but two, one at low shear rates and the other at high shear rates, and a Newtonian region at intermediate shear rates. This behavior was first reported by Onogi and Asada [19] and it has also been observed in polymeric liquid crystals formed by rigid cylindrical molecules [19–21], in AOT/water lamellar liquid crystals [18] and in elongated micellar solutions of cetyltrimetylammonium tosilate [22, 23].

For concentrations that exceed the second maximum, the coexistence of the Lam_1 and Lam_2 phases modifies substantially the rheological behavior. In this case, for a 60 wt% sample, a thixotropic loop forms at low shear rates and this changes into an antithixotropic loop at higher shear rates (Fig. 11D). The area of this thixotropic loop increases with increasing surfactant concentration, and within the concentration range corresponding to the third peak in the viscoelastic properties (80–90 wt%), close to the point where a single Lam_2 phase appears, the viscosity loops become almost thixotropic with a near power law in the ascending mode and an inflection in the descending mode (Fig. 11E). When a second cycle is applied to the same sample, the thixotropic area shrinks and a very small antithixotropic cycle appears at high shear rates (not shown).

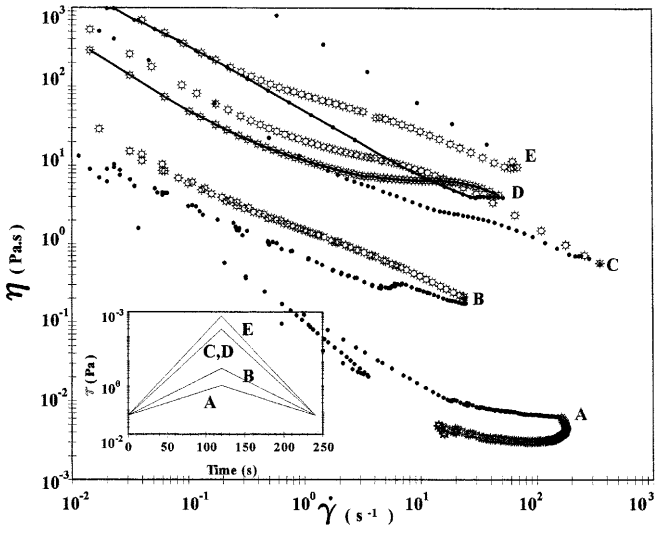

Fig. 11 Viscosity as a function of shear rate in an exponentially increasing and decreasing stress program applied to *A* 1 wt% (0.06–1 Pa), *B* 3 wt% (0.06–5 Pa), *C* 20 wt% (0.06–300 Pa), *D* 60 wt% (0.06–200 Pa) and *E* 90 wt% (0.06–700 Pa) DDAB samples. Increasing stress mode (●) and decreasing stress mode (✲)

Discussion

Low-concentration regime

Two transitions were detected at low concentrations in the DDAB/water system by a battery of techniques. The concentrations where the transitions are observed depend slightly on the method used to detect them (Table 1).

Surface tension data suggest aggregation at the first "break" (Fig. 1); moreover, the surface tension decreases with a smaller slope above this break indicating that the concentration of free DDA^+ increases slightly with increasing DDAB concentration in agreement with data extracted from ion-selective-electrode measurements (Fig. 3). Sudan III solubilization measurements also demonstrate the formation of aggregates at the first transition (Fig. 1). Rhodamine 6G tests indicate that there are no aggregates below the first transition and that they form above it. Moreover, turbidity (measured at 600 nm) increases rapidly with increasing concentration above the first transition, indicating that vesicles instead of micelles form, since the latter are too small to be detected by this technique. The large increase in the Sudan III solubilization capacity of the aggregates (Fig. 1) and the large increase in the slope of the plot of the relative viscosity versus ϕ_{nom} at the second

transition (Fig. 4) indicate structural changes and growth at this concentration.

McNeil and Thomas [24] did not find any transition by conductimetry; however, our conductivity data clearly show a break at concentrations around 0.03 mM (Fig. 2). The plot of Λ versus $\sqrt{c}$ establishes that the aggregates at the first transition are less conductive than the monomeric species, as expected (inset in Fig. 2). Similar results were reported for solutions of long-chain dialkylammonium chlorides [25], of long-chain pyridinium salts [26] and for mixtures of surfactant and alcohol [27].

In the plot of Λ versus $\bar{c}$ (inset in Fig. 2), two plateaus, two drops and an intermediate zone with small slope, were detected. This method was proposed for micelles [31, 32] and it has never been applied to vesicles; however, from the results discussed later, it appears that it is also valid for vesicles. The flatness of the first plateau ($c <$ cvc) has been interpreted as evidence for the absence of dimers and other oligomers – or at least that these species are not present in appreciable concentrations [28–31]. The sharp drop after the first plateau signals the formation of aggregates with a high aggregation number ($n = 491$). To estimate n and the aggregation number in the external ($n_{ext} = 305$) and internal ($n_{int} = 186$) layers, the assumption that vesicles are spherical and the data of Matsumoto [32] (diameter of 10 nm with a single bilayer of 4.1-nm thickness) were used.

The value of Λ_d in the intermediate zone has been interpreted as the molar conductivity of the aggregates, Λ^{agg}, including their diffuse ionic double layers [29, 31]. At the beginning of the intermediate zone, $\Lambda^{agg} = 28$ S cm^2 mol^{-1} (inset in Fig. 2). This value is bigger than of micelles of dodecylammonium trifluroacetate (10 S cm^2 mol^{-1}) [30] and of sodium dodecyl sulfate [29], which confirms that vesicles are more conductive than micelles. However, as the vesicles grow, their differential equivalent conductivity decreases because both the amount of surfactant in the internal layer and the volume of the internal aqueous solution containing Br^- and DDA^+ increase. For instance, assuming a single bilayer and using the data of Matsumoto [32] for vesicles at the beginning (10 nm) and at the end (22 nm) of the intermediate zone, it is found that the ratio of surfactant in the internal layer to the total surfactant increases from 35.6 to 42.2% as the vesicles grow from 10 to 22 nm; the volume of the aqueous solution inside the vesicles also increases from 0.58 to 24.7% of the total volume of the vesicles in the same concentration interval. Both processes clearly reduce the concentration of charge carriers [33] and, hence, the conductivity of the vesicles.

The second drop in the plot of Λ_d versus $\bar{c}$ is less abrupt and corresponds to the gradual transformation of small unilamellar vesicles into larger multilamellar liposomes. Matsumoto [32] reported liposomes of 215 nm at the end of the second plateau, in agreement with our interpretation.

In the high concentration plateau, $\Lambda_d = \Lambda^{agg} \approx 0$ (inset in Fig. 2). This indicates that the giant liposomes contribute very little to the total conductivity of the system; however, this does not necessarily imply that the liposomes are not charged. From the arguments made previously, it is clear that the giant liposomes are poor conductors because the amount of DDAB in the external layer is only a small fraction of the total surfactant concentration and the internal aqueous volume is a large portion of the total volume of the liposomes.

Other evidence that vesicles near the cvc are highly conductive comes from ion-selective-electrode measurements. The estimated degree of ionization of the vesicles is larger ($\alpha \approx 0.5$) than those for alkyltrimethylammonium bromide micelles ($\alpha \approx 0.19$–0.3) [34–37]. Zana [38] estimated α for a series of n-alkyldodecyldimethylammonium bromide micelles as a function of the alkyl group chain length ($n = 2$–10) by conductimetry and Br^--selective-electrode potentiometry, with the assumption that the concentration of free surfactant ions remained constant above the critical micelle concentration, and found that α increases with increasing chain length. Extrapolation of Zana's data to $n = 12$ (DDAB) gives $\alpha = 0.74$ from ion-selective-electrode measurements and 0.87 from conductimetry, which corroborate our results; however, McNeil and Thomas [24] estimated from conductivity measurements that $\alpha \approx 0$ for DDAB vesicles near the cvc and explained their results in terms of the low curvature of the interface. Our results appear to be inconsistent with a flat interface; however, Matsumoto [32] showed by small-angle X-ray scattering that the vesicles have a very rough surface. In fact, he estimated that the surface area of the vesicles is 5 times larger than that of a smooth sphere of similar diameter. Also, Matsumoto [39] reported that the micellar surface area of $C_{12}E_8$ was only twice as large as that of a smooth sphere of equivalent diameter. Hence, the greater surface area of the rugged vesicles and the large volume of the hydrocarbon tails allow a larger separation among the polar heads, reducing the surface electrical potential and, consequently, the attraction of the counterions.

In summary, as for other double-tail surfactants, DDAB has the tendency to aggregate in structures with curvature close to zero, i.e., vesicles and lamellae, because of its high surfactant packing parameter [$v/(al_c) \approx 0.62$)] [7]. In fact, DDAB forms small unilamellar vesicles and not micelles at concentrations between 0.012 and 0.086 mM, depending on the sensitivity of the method used (Table 1). The second transition, detected between 0.36 and 0.66 mM, corresponds to the gradual growth of the vesicles, which leads to the formation of giant multilamellar liposomes.

Vesicles at the cvc are highly conductive but they become less conductive with increasing DDAB concentration because the concentration of carriers (free ions) decreases as the vesicles grow.

High concentration regime

In this regime, the rheological behaviour is complex and rich: samples exhibit non-Newtonian behavior, viscoelasticity, yield stresses and time-dependent flow. Non-Newtonian behavior is detected in the 1 wt% sample, contrary to the findings of Matsumoto et al. [1]; this discrepancy may be due to differences in the sensitivity of the rheometers employed. The biphasic aqueous dispersion of liquid crystals shows power-law behavior and thixotropy but no yield stresses (Fig. 11A). Increasing the DDAB concentration within this biphasic region changes the rheological response drastically. The 3 wt% DDAB sample depicts yield stresses (Fig. 6) and antithixotropy in exponentially increasing and decreasing stress cycles with a power-law behavior in the ascending mode and the three regions of Onogi and Asada [19] in the decreasing mode (Fig. 11B). Moreover, at this concentration, the elastic and loss moduli as well as the complex viscosity pass through a maximum (Fig. 8). Even though the 1 and 3 wt% samples are located in the same biphasic region, the rheological differences suggest subtle structural differences between these two samples. For biphasic aqueous dispersions of AOT liquid crystals, Alexopoulos et al. [40] reported abrupt changes in surface tension, viscosity and turbidity at a concentration of 7.5 ± 0.5 wt%, which they attributed to a phase inversion from aqueous–continuous to liquid-crystalline–continuous dispersions. Similar interpretation can be given to the differences in the rheological properties observed here. In fact, Matsumoto et al. [1] observed an ordered and birefringent continuous phase with some spherulites in the concentration range 3–4 wt% and only Maltese crosses dispersed in an isotropic, nonbirefringent medium in the 1 wt% sample. Also, the rheological behavior of the 3 wt% DDAB biphasic sample is quite similar to those of the 10 wt% (Fig. 10) and 20 wt% one-phase Lam_1 samples (Figs. 8, 11), which substantiates the phase-inversion hypothesis.

Another maximum in the rheological properties (Fig. 8 and Ref. [1]) is depicted between 15 and 20 wt% within the Lam_1 region. Yield stresses are also detected by creep-flow experiments (Fig. 6) and oscillatory measurements in a controlled-stress rheometer (Fig. 7). The time-dependent flow behavior is totally antithixotropic and the three regions of Onogi and Asada are observed in both ascending and descending modes (Fig. 11C). Notice also that the shear viscosity is 2 orders of magnitude larger than that in the 3 wt% biphasic dispersion (cf. Fig. 11B, C). This is consistent with the observations of Matsumoto et al. [1] that a different (stripelike) structure develops in this concentration range.

The third maximum in the rheological properties is observed at the onset of the Lam_2 phase boundary (Fig. 8). This phase has a much finer texture than that of the Lam_1 phase [3]. The time-dependent flow behavior is now thixotropic (Fig. 11E) in contrast to the antithixotropic behavior exhibited by Lam_1 samples (Figs. 10, 11C). Yield stresses are also detected in the Lam_2 region. Of course, the rheological properties in the biphasic (Lam_1/Lam_2) region reveal features of both phases (Fig. 11D).

At this point it is interesting to contrast the rheological behavior of the Lam_1 and Lam_2 phases. Samples in both Lam_1 and Lam_2 regions behave as physical gels, i.e., $G' > G''$ and both are fairly independent of frequency (Fig. 7A) and temperature above the Kraft point (Fig. 9). In as much as G' of the Lam_2 samples is almost 2 orders of magnitude larger than G' of the Lam_1 samples, the density of the structural network points must be much higher in the former. Upon application of increasing and decreasing stress cycles, a structure is built up in the Lam_1 samples which results in antithixotropy (Figs. 10, 11C), whereas thixotropy is observed in Lam_2 samples because of structure breakdown (Fig. 11E). In fact, Goldszal et al. [41] presented conclusive evidence from polarizing microscopy, transmission electron microscopy and rheometry that shear flow modifies and induces structure in AOT/water liquid-crystalline samples. DDAB/water samples also showed different textures and appearances after being sheared [17]. Hence, the different rheological behavior of the Lam_1 and Lam_2 phases may be attributed to the differences in the structural network point densities, although other parameters, such as the number density of defects, may also play a role.

Bergmeier et al. [42] observed strong elastic properties and yield stresses in multilamellar systems of cationic surfactants. Time-dependent phenomena are observed as the solution is sheared. The flow leads to a strong increase in the storage modulus and in the yield stress value. The steady state is attained on time scales of the order of 1 hour, and the resulting elasticity is proportional to the magnitude of the shear rate. Such behavior is explained by the stripping off of vesicle shells, which leads to a buildup of the new and smaller vesicles. By shearing, a permanent modification has been imposed on the system, reducing the polydispersity of vesicles.

The strong increase in the storage modulus observed by Bergmeier et al. may be related to the presence of antithixotropy, as observed in Fig. 11B and C. In fact, the hysteresis observed in the unsteady-state curves of Fig. 11B and 11C is a manifestation of a more structured fluid, since the viscosity in the decreasing

stress mode is higher than that in the increasing mode. This observation implies that the storage modulus of the system has increased with the shear rate.

Additional evidence of changes in the structure of the fluid as the shear rate is modified in lyotropic lamellar phases has been given by Diat and Roux [43] and by Roux et al. [44]. These authors have described an orientation diagram for lamellar phases under non-equilibrium conditions that demonstrates that different and permanent phases can be produced under shear. In this regard, increasing the final stress or applying consecutive cycles leads to different rheological behavior due to permanent (or long-lived) microstructural changes, in agreement with the results reported in the previously cited papers: a lamellar phase is transformed into a very stable, long-lived multilayered vesicular system. In fact, for certain values of the shear rate, the lamellar phase organizes itself into spherical multilayer vesicles of well-controlled size. The size is shown to vary as the inverse of the square root of the shear rate [45].

Observations of the orientation states that lyotropic phases take under shear [44] reveal that the transition at which the layers organize themselves into multilayered vesicles corresponds to a change in the slope of the shear stress versus shear rate curve in the steady state. A second slope change is identified with the transition into parallel layers with no vesicles. If, however, measurements are made under non steady-state conditions (not waiting for the complete steady-state equilibrium), a thixotropic cycle is observed. Similar results are presented in Fig. 11A and E.

The electrical conductivity also shows complex behavior in the high concentration regime (Fig. 8). Similar behavior was reported for AOT/water lamellar liquid crystals [46, 47]. Nevertheless, this behavior has not been explained yet.

At low concentrations, the conductivity increases with increasing DDAB concentration as expected from the ionic nature of this surfactant. This behavior is observed up to 7–8 wt% DDAB, well into the Lam_1 region; however, samples are more fluid above 3 wt% and up to 7–8 wt% DDAB as is evident from the smaller moduli (Fig. 8) and shear viscosity [1], which allows a faster conduction of ions through the water channels of the liquid crystals. Also, the presence of dispersed conductive particles at these concentrations [1], contributes to the total conductivity by electrophoretic conduction.

The drop in conductivity with increasing surfactant concentration above about 10 wt% DDAB can be anticipated because of the nature of the lamellar phase, which can be thought of as a randomly oriented arrangement of conductive water channels in a nonconductive medium; however, the rise in conductivity at 25 wt% DDAB is unexpected. In lamellar phases, the total conductivity depends on the relative thickness of the water layers (d) and on the Debye length, κ^{-1}. When $d > 2\kappa^{-1}$, the presence of the lamellae decreases the effective specific surface area available for conduction and increases the effective specific length because of tortuosity of the water channels and defects among the liquid-crystalline microdomains. These two effects tend to reduce the total specific conductivity of the system. The total specific conductivity, κ_T, is related to the specific conductivity of the interlamellar aqueous solutions, κ_0, by

$$\kappa_T = \varsigma \Phi_w \kappa_0 \ . \tag{1}$$

Here Φ_w is the volume fraction of the interlamellar aqueous solution in the system and ς is a tortuosity factor. Under these conditions, κ_T should decrease with increasing surfactant concentration (see Fig. 8 for DDAB concentrations between 10 and 25 wt%); however, when $d \leq 2\kappa^{-1}$, the concentration of counterions increases as a consequence of the overlapping of the ionic double layers of the charged surfaces in the water channels, resulting in an increase in κ_T with surfactant concentration. Moreover, under these circumstances, the surface conductivity, κ_S, also contributes strongly to κ_T [11]. Hence, the total conductivity should increase as the concentration of surfactant increases (see Fig. 8 for DDAB concentrations higher than 25 wt%) according to [11]

$$\kappa_T = \kappa_0 + (S_l/V_l)\kappa_S \ . \tag{2}$$

Here S_l and V_l are the surface area and the volume per unit length of a capillary channel. This phenomenon is known as "capillary superconductivity" [11].

For lamellae channels, $S_l/V_l \approx 2/d$. The value of d can be estimated when the thickness of the lamellae, D, the concentration of surfactant and the molar volumes of water and surfactant are known. For the Lam_1 phase, $D = 2.3$ nm [3].

To estimate κ_0, we assume that capillary superconductivity begins at the concentration where the conductivity goes through a minimum (about 25 wt%) and that at this concentration, the ionic atmospheres of the opposite surfaces touch each other, i.e., $d/2 = \kappa^{-1} = 1/B\sqrt{I}$. Here I is the ionic strength, which is basically due to the contribution of Br^-, and $B(\equiv [8\pi N_A e_0^2/1000kT\varepsilon]^{1/2})$, where N_A is Avogadro's number, e_0 is the electronic charge, k is the Boltzmann constant and ε is the permittivity. At 25 °C, $B = 8.291 \times 10^7$ cm^{-1}. Once I is known, κ_0 can be calculated using Debye–Hückel–Onsager theory [48] as follows:

$$\kappa_0 = \lambda_{Br^-}[Br^-]/1000 \tag{3}$$

and

$$\lambda_{Br^-} = \lambda_{0,Br^-} - (A + B\lambda_{0,Br^-})\sqrt{I} \ . \tag{4}$$

Table 2 Total (κ_T) and interlamellar solution (κ_0) conductivities, aqueous layer thickness (d), bromide concentration in the interlamellar layer ([Br^-]) and degree of ionization (α) as a function of didodecyldimethylammonium bromide (*DDAB*) concentratrion (c_{DDAB})

c_{DDAB} (wt%)	κ_T (mS/cm)	$d \times 10^6$ (cm)	κ_0 (mS/cm)	[Br^-] (M)	α
6	0.91	2.20	0.206	0.0031	0.024
7.5	0.92	1.85	0.218	0.0033	0.02
10	0.90	1.20	0.232	0.00035	0.016
15	0.85	0.757	0.234	0.00351	0.011
20	0.76	0.534	0.216	0.00324	0.007
25	0.72	0.40	0.235	0.0023	0.0042
30	0.81	0.312	0.186	0.00258	0.004
35	0.92	0.251	0.145	0.002	0.0027

Here λ_{Br^-} and λ_{0,Br^-} are the bromide ion conductivities at the given concentration and at infinite dilution, respectively, and A is $82.4(\varepsilon T)^{-1/2}\eta_s^{-1}$) and B is $8.2 \times 10^{-5}(\varepsilon T)^{-3/2}$, with ε and η_s being the dielectric constant and the viscosity of water, respectively. With this procedure, we estimated $\kappa_0 = 2.35 \times 10^{-4}$ S cm^{-1} at the minimum. Then, with Eq. (2), we calculated $k_S = 9.72 \times 10^{-11}$ S. In common glass filters, κ_S is around 10^{-9} S [13] and in isolated lamellae foam stabilized with sodium dodecyl sulfate with or without salt, k_S is of the order of $(2.5-7.5) \times 10^{-9}$ S [49, 50]. Also, from the value of k_0, the concentration of free Br^- in the interlamellar solution can be estimated. For 25 wt% DDAB concentration, α is 0.0042.

For a randomly oriented arrangement of conductive channels in a nonconductive medium, $\varsigma = 0.33$. Using this value for the lamellae and assuming that ς and k_S do not vary with DDAB concentration, which may not be necessarily true, k_0 and α can be calculated as a function of surfactant concentration. Both k_0 and α decrease with increasing DDAB concentration (Table 2). Extrapolation of α to low DDAB concentrations yields a value similar to that estimated by ion-selective-electrode potentiometry ($\alpha = 0.5$).

In summary, the rheological and conductivity behavior in the high concentration regime is complex. Maxima and minima in rheological material functions and in conductivity are related to structural changes and phase transitions. In exponentially increasing and decreasing stress cycles, the rheological response shifts from thixotropic to antithixotropic or vice versa, depending on the DDAB concentration and the level and duration of the final applied stress. The conductivity rise above 25 wt% DDAB in the Lam_1 phase region can be qualitatively explained by the capillary superconductivity theory.

Acknowledgements This work was supported by the Consejo Nacional de Ciencia y Tecnología de México (grant nos. 3397-E and 3343-E). F.B. recognizes the support of CONACYT.

References

1. Matsumoto T, Hieuchi T, Horie K (1989) Colloid Polym Sci 267:71–79
2. Matsumoto T, Ito D, Kohno H (1989) Colloid Polym Sci 267:946
3. Fontell K, Ceglie A, Lindman B, Ninham B (1986) Acta Chem Scand A 40:247
4. Chen SJ, Evans DF, Ninham B (1984) J Phys Chem 88:1622
5. Chen SJ, Evans DF, Ninham B, Mitchel DJ, Blum FD, Pickup S (1986) J Phys Chem 90:842
6. Chen V, Evans DF, Ninham B (1987) J Phys Chem 91:1823
7. Warr GG, Sen R, Evans DF, Trend JE (1988) J Phys Chem 92:774
8. Dubois M, Gulik-Krzywicki T, Cabane B (1993) Langmuir 9:673
9. Caboi F, Monduzzi M (1996) Langmuir 12:3548
10. Morris ER (1984) In: Phillips GO, Wedlock DJ (eds) Rheology of hydrocolloids. Gums and stabilisers for the food industry 2. Proceeding of the 2nd International Conference Held at Wrexham, Clywd, Wales. Pergamon, New York, pp 57–78
11. Schukin ED, Pertsov AV, Amélina EA (1988) In: Schukin ED (eds) Química coloidal. MIR, Moscow, pp 220–221
12. Schulz PC (1989) Colloids Surf 34:64
13. Morini MA, Schulz PC (1997) Colloid Polym Sci 275:802
14. Gruen DWR (1985) J Phys Chem 89:146
15. Cartmell E, Fowles GWA (1964) Valencia y estructura molecular. Reverté, Barcelona
16. Ferry JD (1980) Viscoelastic properties of polymers. Wiley, New York
17. Soltero JFA (1995) Ph D thesis. Universidad Nacional Autónoma de México
18. Soltero JFA, Robles-Vásquez O, Puig JE, Manero O (1995) J Rheol 39:235
19. Onogi S, Asada T (1980) In: Astarita G, Marrucci G, Nicolas L (eds) Rheology, vol 2. Plenum New York, pp 127
20. Berry GC (1976) Properties of rigid chain polymers in diluite and concentrated solutions. Eighth Biennial Polymer Symposium. Division of Polym Chem Am Soc, Key Biscayne; Kulichikhin VG, Malkin AY, Papkov SP (1984) Polym Sci USSR 26:499–524
21. Wissburn KF (1981) J Rheol 25:619
22. Bautista F, De Santos JM, Puig JE, Manero O (1999) J Non-Newtonian Fluid Mech 80:93–113
23. Soltero JFA, Bautista F, Puig JE, Manero O (1998) Langmuir 15:1604–1612
24. McNeil R, Thomas JK (1980) J Colloid Interface Sci 73:522
25. Ralston AW, Eggenberger DN, Brown PL (1948) J Am Chem Soc 70:977
26. Brown GL, Grieger PF, Evers EC, Klaus CA (1947) J Am Chem Soc 69:1835
27. Evers EC, Grieger PF, Klaus CA (1946) J Am Chem Soc 68:1137
28. Hartley GS (1936) Aqueous solutions of paraffin chain salts. Herman et Cie, Paris
29. Stiger D (1954) Recl Trav Chim Pays-Bas 73:611
30. Sugihara G, Era Y, Tunatsu M, Kunitake T, Lee S, Sasaki Y (1987) J Colloid Interface Sci 187:435
31. Asakawa T, Shiraishi T, Sunasaki S, Muyaguishi S (1995) Bull Chem Soc Jpn 68:2503

32. Matsumoto T (1992) Colloid Polym Sci 270:492–497
33. Schönfelder, Hoffmann H (1994) Ber Bunsenges Phys Chem 98:842
34. Anacker EW, Ghose HM (1963) J Phys Chem 67:1713
35. Anacker EW, Westwell AE (1994) J Phys Chem 68:3490
36. Zana R (1980) J Colloid Interface Sci 87:330
37. Lianos P, Zana R (1983) J Phys Chem 87:1289
38. Zana R (1980) J Colloid Interface Sci 78:330
39. Matsumoto T (1990) Ber Bunsenges Phys Chem 94:827
40. Alexopoulos A, Puig JE, Franses EI (1989) J Colloid Interface Sci 128:26
41. Goldszal A, Jaimeson AM, Mann JA, Polak J, Rosenblatt Ch (1996) J Colloid Interface Sci 180:261–268
42. Bergmeier A, Gradzielski M, Hoffmann H (1998) J Phys Chem 102:2838
43. Diat O, Roux D (1993) J Phys France 3:1427
44. Roux D, Nallet F, Diat O (1993) Europhys Lett 24:53
45. Diat O, Roux D, Nallet F (1993) J Phys II 3:1427
46. Ekwall P, Mandell L, Fontell K (1970) J Colloid Interface Sci 33:215
47. Fontell K (1973) J Colloid Interface Sci 44:318
48. Robinson RA, Stokes RH (1959) Electrolyte solutions. Academic Press, New York
49. Clunie JS (1967) Trans Faraday Soc 63:505
50. Swayne EN, Newman J, Radke CJ (1998) J Colloid Interface Sci 203:69